

NACA RM L57H22

**CONFIDENTIAL**

Copy 5  
RM L57H22

UNCLASSIFIED

c.2



# RESEARCH MEMORANDUM

TRANSONIC FLUTTER INVESTIGATION OF ARROWHEAD WING WITH  
TIP AILERONS AND TRAILING-EDGE FLAPS

By George W. Jones, Jr., and Robert W. Boswinkle, Jr.

Langley Aeronautical Laboratory  
Langley Field, Va.

**CLASSIFICATION**

To **UNCLASSIFIED**

**LIBRARY COPY**

NOV 4 1957

By authority of

LANGLEY AERONAUTICAL LABORATORY  
LIBRARY, NACA  
LANGLEY FIELD, VIRGINIA

CLASSIFIED DOCUMENT

This material contains information affecting the National Defense of the United States within the meaning of the espionage laws, Title 18, U.S.C., Secs. 793 and 794, the transmission or revelation of which in any manner to an unauthorized person is prohibited by law.

## NATIONAL ADVISORY COMMITTEE FOR AERONAUTICS

WASHINGTON  
November 4, 1957

**CONFIDENTIAL**



## NATIONAL ADVISORY COMMITTEE FOR AERONAUTICS

## RESEARCH MEMORANDUM

TRANSONIC FLUTTER INVESTIGATION OF ARROWHEAD WING WITH  
TIP AILERONS AND TRAILING-EDGE FLAPS

By George W. Jones, Jr., and Robert W. Boswinkle, Jr.

## SUMMARY

A transonic flutter investigation has been made of models of the wing of a new fighter airplane. The models were dynamically and elastically scaled by criteria which provide a flutter safety margin. The wing had an arrowhead plan form, was equipped with ailerons at the tips and with flaps at the trailing edges, and was cantilever mounted. The investigation was made in the Langley transonic blowdown tunnel for a Mach number range from about 0.75 to 1.35.

The basic configuration was flutter free at Mach numbers from about 1.0 to 1.1 at simulated altitudes as low as sea level, but flutter was obtained at altitudes above sea level at both higher and lower Mach numbers. The flutter mode at subsonic Mach numbers involved primarily bending and torsion of the wing with little independent aileron motion. The flutter mode at supersonic Mach numbers involved primarily aileron rotation with some bending of the aileron spar, and the flutter boundary was such that a rapid decrease in dynamic pressure required for flutter was obtained at a Mach number of about 1.1.

In an effort to improve the flutter boundary at supersonic Mach numbers, three aileron modifications were investigated. Increases in the stiffness of the aileron spar reduced the altitude at supersonic Mach numbers at which flutter occurred. Cutting off the tip of the aileron or increasing the simulated actuator stiffness to about three times the original value eliminated flutter at supersonic Mach numbers at altitudes as low as sea level.

An intensive investigation of the flutter boundary at Mach numbers from about 0.85 to 0.95 was made with the ailerons of the basic configuration in an undeflected, locked position. The data obtained indicated that the flutter in this Mach number region ceases if the dynamic pressure is increased sufficiently. Aileron restraint was not indicated to have much effect on the subsonic flutter characteristics.

[REDACTED]

## INTRODUCTION

The transonic flutter characteristics of the wing of a new fighter airplane have been studied in the Langley transonic blowdown tunnel with dynamically and elastically scaled models. The results obtained were thought to be of enough general interest to warrant publication.

The wing had an arrowhead plan form, was equipped with ailerons at the tips and with flaps at the trailing edges, and was cantilever mounted. Modifications of the ailerons of the basic configuration were studied in an effort to obtain adequate safety from flutter at altitudes as low as sea level in the low supersonic Mach number range. The investigation was made at Mach numbers from about 0.75 to 1.35.

## SYMBOLS

$b_a$	average streamwise semichord of exposed panel, ft
$b_s$	average streamwise semichord of streamwise strip, ft
$EI$	bending stiffness, lb-ft <sup>2</sup>
$f_f$	flutter frequency, cps
$GJ$	torsional stiffness, lb-ft <sup>2</sup>
$I_s$	moment of inertia of streamwise strip about lateral axis through strip center of gravity (fig. 1), slug-ft <sup>2</sup>
$k_\beta$	stiffness of simulated aileron actuator, ft-lb/radian
$l$	length scale factor, $\frac{\text{Typical length of model}}{\text{Corresponding length of airplane}}$
$m$	mass scale factor, $\frac{\text{Typical model mass}}{\text{Corresponding airplane mass}}$
$m'$	mass of exposed panel, slugs
$m_s$	mass of streamwise strip, slugs
$M$	Mach number

q	dynamic pressure, lb/sq ft
t	time scale factor, $\frac{\text{Time for tunnel airstream to move 1 model wing-chord length}}{\text{Time for airplane to move 1 airplane wing-chord length}}$
T	static temperature, $^{\circ}\text{R}$
v	volume of frustum of cone, having a base diameter equal to the streamwise root chord and having a tip diameter equal to the streamwise tip chord, cu ft
V	velocity, fps
$\bar{V}$	reduced velocity based on a representative natural frequency, $\frac{V}{b_a \omega}$
$x_{cg}$	center-of-gravity location of streamwise strip, percent streamwise chord from leading edge
$\delta_s$	width of streamwise strip, ft
$\eta$	stiffness reduction factor used to provide margin of safety in application of model flutter test results to the airplane
$\mu$	mass ratio, $m'/\rho v$
$\rho$	static air density, slugs/cu ft
$\omega$	representative natural frequency, radians/sec
$\omega_f$	flutter frequency, $2\pi f_f$ , radians/sec
$\omega_\alpha$	measured frequency of vibration mode having, predominantly torsion motion, radians/sec

## Subscripts:

A	airplane
M	model

## MODELS

### Configurations

The basic models investigated were 0.04-size, dynamically and elastically scaled versions of the wing of a new fighter airplane. A sketch and photographs of one of the basic models are shown in figures 1 and 2, respectively. Some of the model geometric properties are listed in table I.

The wings had an arrowhead plan form with  $55^\circ$  sweepback at the leading edge and  $10^\circ$  sweepback at the trailing edge. The airfoil sections were NACA 65A003 sections in the streamwise direction. The hinge line of the tip ailerons intersected the aileron root chord (the chord which includes the innermost parting line, fig. 1) at the 56-percent-chord station. The ratio of aileron area to exposed wing area was 0.200. The aileron-actuator stiffness was simulated by springs (fig. 2(b)) attached to the wing and to the ailerons upstream of the hinge line. Each flap was attached to the wing by means of two flexure hinges (fig. 1). The stiffness of the flexure hinges simulated the flap-control stiffness of the airplane for the flaps in the undeflected, locked position. All the ailerons and flaps were tested in the undeflected position with the wings at zero angle of attack.

Three wing models, designated wings 1, 2, and 3, were used in the investigation. The three wings were used to study other configurations in addition to the basic one. A complete list of the configurations investigated is given in table II. For some configurations only one wing panel is listed in table II as having been investigated; in such cases the opposite wing panel was present but the aileron was either restrained in rotation or was removed.

All the models were meant to be identical, except for those cases (table II) where the ailerons were purposely modified. However, as shown subsequently in the "Physical Properties" section of this report, differences in the models did exist.

### Scaling

In scaling the airplane properties it was required that the non-dimensional mass and stiffness distributions should be the same for the model as for the airplane. The mass and stiffness levels for the model were obtained by specifying the scale factors for the fundamental quantities involved: length, mass, and time.

The size of the model was chosen from tunnel-wall-interference considerations to be about the maximum permissible value in arriving at a length scale factor of

$$\lambda = 0.04 \quad (1)$$

The mass scale factor was obtained from a requirement that the mass ratio  $\mu$  should be the same for the model as for the airplane, which results in

$$m = \frac{\rho_M}{\rho_A} \lambda^3 \quad (2)$$

In order to locate simulated sea-level altitude in the tests near the middle of the tunnel density range available at a Mach number of 1, the density ratio was chosen to be  $\rho_M/\rho_A = 2.00$ . This location of simulated sea-level altitude allows altitudes below sea level to be obtained and makes it possible to indicate flutter margins for cases wherein flutter does not occur above sea level.

The time scale factor was obtained from a requirement that the reduced velocity  $\bar{V}$  should be the same for the model as for the airplane, which results in

$$t = \left( \frac{V_M}{V_A} \right)^{-1} \lambda$$

Since the Mach number is the same for the model as for the airplane, the time scale factor may be written as

$$t = \left( \frac{T_M}{T_A} \right)^{-\frac{1}{2}} \lambda \quad (3)$$

The static temperature for the airplane  $T_A$  is a function only of altitude, and for sea-level altitude it was taken to be  $519^\circ$  R. However, in the tunnel during a run the temperature continually drops as air is expended from the reservoir and the temperatures obtained at the various flutter points during an investigation are different. A study of previous flutter data indicated that  $408^\circ$  R was near the average value of the static temperature that would be expected during the present runs, and this value was used to obtain the temperature ratio used in scaling  $T_M/T_A = 0.786$ .

A list of the pertinent wing and flow quantities and the design scale factors used is given in table III. It may be noted that the factor  $\eta$  is used in the scale factors for some of the quantities in table III. The factor  $\eta$  has the value 0.76 and occurs because the stiffnesses of the model were made 76 percent of those which would result from application of the scale factors as specified (eqs. (1), (2), and (3)). The purpose of reducing the model stiffnesses was to provide a margin of safety in the application of the model flutter test results to the airplane. It may be noted that the stiffness reduction results in the design reduced velocity for the model being equal, not to that of the airplane, but to that of an airplane having stiffnesses 76 percent of those of the actual airplane.

Because the temperature during a run is not a controllable quantity, the exact value of the design reduced velocity  $\bar{V}$  (through use of eq. (3)) is not obtained. The two quantities which are controllable during a run are dynamic pressure and Mach number. If the dynamic pressure and Mach number are considered to be held constant, a change in temperature results in a change in density and velocity. Thus, the consequence of having a temperature during a run different from the design temperature is that neither the reduced velocity nor mass ratio is exactly simulated. However, a combination of reduced velocity and mass ratio, which can be expressed in terms of the dynamic pressure

$$\frac{\bar{V}_M^2}{\mu_M} \propto q_M$$

is independent of the temperature, and this combination is exactly simulated in the tests by the expedient of interpreting the simulated altitude in terms of dynamic pressure. Thus, the scale factor in table III for dynamic pressure is used to convert the dynamic pressure for the airplane at any altitude and Mach number to the dynamic pressure for the model at the same altitude and Mach number. The dynamic pressure for the airplane is assumed to be that of the ICAO standard atmosphere (ref. 1). It may be noted that for a given altitude  $q/M^2$  is a constant quantity.

The effect of not individually satisfying exactly the mass ratio and reduced velocity is believed to be negligible in the present investigation. Experience with a wide variety of flutter models has indicated that, at least within the operational limits of the tunnel, flutter at a given Mach number tends to occur at a constant value of dynamic pressure regardless of the individual values of density and velocity.

### Construction

Construction details of the basic models are included in figure 3. Each wing had a hollow, welded, aluminum-alloy spar with a vertical web at the center of the spar running along the spar length. The ribs were of aluminum alloy and were welded to the spars. The leading edge was made of mahogany. A small piece of aluminum alloy along the rear of the structure furnished a surface for attachment of the flap flexure hinges. The flaps were fabricated of aluminum alloy with lightening holes as indicated in figure 3. Each aileron had a hollow, welded, aluminum-alloy spar to which was fabricated an aluminum-alloy trailing edge and ribs. The leading edge of each aileron was made of mahogany. Balsa was used to fill the voids in the construction of the wings, flaps, and ailerons. Silk cloth was glued to the outer surface. The U-shaped spring (fig. 2(b)), which simulated the rotational stiffness of the aileron actuator, and the aileron and flap flexure hinges were made of steel. The two wing panels were attached to a 0.25-inch-thick solid-aluminum-alloy spar (figs. 1 and 2(b)) which fitted into the mounting block (fig. 2(c)) to form a cantilever mount for the models. Motion of the wing at the root near the trailing edge was restrained by a tab (figs. 1 and 2(b)) attached to the wing which fitted into the mounting block. The mounting block was machined from solid aluminum alloy.

### Physical Properties

The natural vibration frequencies and node lines for the various configurations are presented in figure 4. These data were obtained by exciting the models with an electromagnetic shaker with the shaker stem located as indicated in figure 4. Salt crystals sprinkled on the wing during resonant vibrations depicted the node lines. The predominant characteristic of each of the first four vibration modes of the basic models (figs. 4(a) and 4(b)) in order of their occurrence was: first bending, second bending, first torsion, and aileron rotation.

Also indicated in figure 4 is the stiffness  $k_{\beta}$  of the aileron-actuator spring for each configuration. The quantity  $k_{\beta}$  was obtained by applying a torque about the aileron hinge line near the forward parting line and measuring the angular rotation of the aileron; during these measurements, deflection of the wing was prevented by clamping the wing to a rigid surface.

Structural influence coefficients were measured on the left panel of wing 2 with the basic aileron configuration. The 18 points at which the measurements were made are indicated in figure 3. The procedure

used is described in reference 2. The values of the influence coefficients as measured after being normalized for unit loads are given in table IV(a). The matrix of table IV(a) was made symmetrical about the diagonal by averaging the corresponding terms. The resulting symmetrical matrix of influence coefficients is presented in table IV(b). The amount by which the terms were adjusted to make them symmetrical is an indication of the accuracy of the measurements. Of the off-diagonal terms measured, 83 percent were within 2 percent of the averaged values, 95 percent were within 4 percent of the averaged values, and the remaining 5 percent were within 4 to 9.4 percent of the adjusted values.

Certain sections of the panel were assumed to be associated with each of the 18 influence-coefficient points. These sections are indicated in figure 3. The mass and center-of-gravity location of each section were determined after the flutter tests by sawing each section out of the left panel of wing 1; these data are given in figure 3. The masses listed were adjusted for the amount of material lost in the saw cuts.

The right panel of wing 1 was sawed into streamwise strips as indicated in figure 1. The mass, center-of-gravity location, and moment of inertia of each strip as corrected for the amount of material lost in the saw cuts are given in table V. It should be noted in figure 1 that the flap was sawed into two pieces. One piece of the flap was attached to strip 2 and the other to strip 4 when the measurements of table V were made. The total mass (table V) of the right panel of wing 1 is about 4 percent greater than that (fig. 3) of the left panel.

The average value of the structural damping coefficient in the first bending mode, as determined for the various models from records of the decay of oscillations induced by plucking the wing, was about 0.02.

#### APPARATUS AND TESTS

The flutter tests were made in the Langley transonic blowdown tunnel which has a slotted test section. The test section is octagonal in cross section and measures 26 inches between flats. During operation of the tunnel a preselected Mach number is set by means of a variable orifice downstream of the test section, and this Mach number is held approximately constant after the orifice is choked while the stagnation pressure, and thus the density, is increased. The static-density range is approximately 0.001 to 0.012 slug per cubic foot and Mach numbers may be obtained from subsonic values to a maximum of about 1.4. It should be noted that, because of the expansion

of the air in the reservoir during a run, the stagnation temperature continually decreases and, thus, the test-section velocity is not uniquely defined by the Mach number. Additional details of the tunnel are contained in reference 3. Excellent agreement between flutter data obtained in the tunnel and in free air has been observed (ref. 4).

In the flutter tests the models were cantilever mounted at zero angle of attack in the mounting block shown in figures 2(a) and 2(c). The mounting block was fitted into a sting in such a way that a 3-inch-diameter fuselage was formed which extended upstream into the subsonic flow region of the tunnel. This arrangement prevented the formation of shock waves off the fuselage nose which might reflect from the tunnel walls onto the model. A sketch of the model mounted on the sting and installed in the tunnel is shown in figure 5. The sting and model weighed approximately 290 pounds, and the system had a fundamental bending frequency of about 15 cycles per second.

Wire strain gages were mounted on the wing spars near the root as sketched in figure 3 so as to indicate model deflections about two different axes. Strain gages were attached also to either the aileron hinge or aileron spring.

The strain-gage signals, the tunnel stagnation and static pressures, and the stagnation temperature were recorded on a recording oscillograph. The strain-gage signals were used to indicate the start of flutter and the flutter frequency. High-speed motion pictures were made during some of the runs and were used in studying the flutter modes. The models were tested at Mach numbers from 0.75 to 1.35 and at simulated altitudes from below sea level up to about 20,000 feet.

## RESULTS AND DISCUSSION

### Presentation of Data

The data obtained in the 37 runs of the present investigation are summarized in table VI. The "Run," "Point," and "Panel behavior" columns of table VI indicate chronologically the events which occurred during each run as the dynamic pressure was being increased. For example, by using the code given in table VI, these columns indicate that in run 1 at point 1 the right panel started to flutter while the left panel was still stable. At point 2 the left panel started to flutter while the right panel continued to flutter. At point 3 both panels ceased to flutter. At point 4 the maximum dynamic pressure obtained during the run was reached and both panels were still stable. In a few of the runs (for example, run 11, table VI) a condition is

indicated which is described in table VI as low damping. In the low-damping regions, intermittent sinusoidal oscillations were obtained which obscured the exact start of definite flutter. The significance of the low-damping regions, as related to the airplane, is not known.

The data of all the runs except runs 36 and 37 are plotted in figures 6 to 11 in the form of dynamic pressure as a function of Mach number. The curved lines on these plots indicate the path followed in approaching the data points.

### Interpretation of Results

As stated in the "Scaling" section of this report, the model stiffnesses were 76 percent of the scaled airplane stiffnesses. The simulated altitudes which are indicated in figures 6 to 11 are thus to be interpreted as altitudes which if cleared by the model could be reached with a 32-percent ( $1/0.76 = 1.32$ ) margin of safety in stiffness by the airplane. This statement assumes, of course, that the model in all other respects exactly simulates the airplane.

An alternate interpretation of the results arises from the fact that for most configurations the dynamic pressure required for flutter varies to a first approximation directly with the stiffness level. Thus, a flutter point obtained with the model indicates that the airplane will flutter at the same Mach number at a simulated altitude corresponding to a dynamic pressure 32 percent higher than that for the model.

### Basic Configuration

The flutter test results (fig. 6) for the basic configuration indicate that at Mach numbers between about 1.0 and 1.1 no flutter was encountered at dynamic pressures corresponding to altitudes as low as about sea level. However, flutter was obtained at altitudes above sea level at both lower and higher Mach numbers.

The flutter obtained at a Mach number of about 0.85, as indicated by a study of the strain-gage and motion-picture records obtained during runs 1 and 5, involved primarily bending and torsion deflections of the entire wing with little independent aileron motion. For the flutter mode the average flutter frequency was 169 cycles per second (table VI). This frequency lies between the frequency of the first vibration mode (fig. 4(a)), which involved primarily a first bending motion of the panel, and the frequency of the second vibration mode, which involved primarily a second bending motion of the panel. The strain-gage and motion-picture records indicated that the flutter in this region was mild. Further evidence pointing to mild flutter was

that the model was not damaged in obtaining the flutter points. An interesting result in run 1 was that a no-flutter region was reached at a dynamic pressure above that required for flutter.

At supersonic Mach numbers two flutter points were obtained (fig. 6) at a Mach number of about 1.15 and two at a Mach number of about 1.3. The flutter frequency (table VI) was around 305 cycles per second, about twice that for the subsonic flutter. The flutter mode, in contrast with that which occurred at subsonic Mach numbers, involved primarily aileron rotation with some bending of the aileron spar; the flutter mode was rapidly divergent and the ailerons were damaged each time flutter was obtained. It may be noted (table VI) that the four supersonic flutter points were obtained with four different panels. In spite of an effort to make the panels identical, they did differ as evidenced by the frequency spectra and actuator-spring stiffnesses (figs. 4(a) and 4(b)). A first-order correction to the dynamic pressure at flutter might be to divide the dynamic pressure by the aileron-actuator stiffnesses (figs. 4(a) and 4(b)); this procedure results in less scatter of the supersonic flutter points. However, regardless of the exact location of the flutter boundary in this region, these data indicate that the dynamic pressure required for flutter decreases very rapidly as the Mach number is increased to above a value of about 1.1.

#### Configurations With Modified Ailerons

As previously noted, the flutter mode at supersonic Mach numbers for the basic configuration involved primarily aileron rotation with some bending of the aileron spar. Therefore, four different modified ailerons were tried in attempts to increase the dynamic pressure required for flutter at supersonic Mach numbers. In the first aileron modification the aileron-spar stiffness was increased by replacing the hollow spar of the basic configuration with a solid one and in the second aileron modification the mass at the tip was reduced by cutting off the basic aileron just outboard of the outboard rib (fig. 3). As indicated in figure 4 some increase in the stiffness of the aileron actuator accompanied the first two modifications. In the third modification the actuator stiffness was increased to about three times the value for the basic configuration. The fourth aileron design incorporated all three modifications.

The results obtained with the modified ailerons are presented in figures 7 to 10. These data indicate that each modification increased the dynamic pressure required for flutter at supersonic Mach numbers above that required for the basic configuration (fig. 6). In fact, the only configuration that still fluttered at altitudes above sea level was the one with the stiffer aileron spar (fig. 7). The flutter

obtained with the modified ailerons at supersonic Mach numbers (fig. 7, runs 11 and 12, and fig. 8, run 16) had somewhat higher frequencies (table VI) than those obtained with the basic configuration.

Flutter was obtained at subsonic Mach numbers with two of the modified aileron configurations (figs. 7 and 10). The flutter mode, as with the basic configuration, involved primarily wing bending and torsion motion with little independent aileron motion. No significance is attached to the fact that no flutter was obtained with the other two modified aileron configurations since the region was not covered intensively.

#### Configurations with Locked Ailerons

The basic configuration was also investigated with the aileron locked to the wing by means of glue along the parting lines and clamps at the leading and trailing edges as indicated in figure 4(g). This arrangement simulates an actuator stiffness which approaches an infinite value and, as might be expected on the basis of the previously discussed results, no flutter was obtained (fig. 11) at supersonic Mach numbers at altitudes down to sea level and below. With this configuration the subsonic region was intensively investigated. At Mach numbers between 0.85 and 0.95 a number of flutter points were obtained and in each case the model became stable as the dynamic pressure was further increased. The flutter mode involved primarily bending and torsion motion of the wing, and the flutter frequency (table VI) was about the same as that for the basic configuration.

The flutter data at a Mach number of about 0.85 for the basic configuration (fig. 6) are noted to be reasonably consistent with those of the locked-aileron configuration (fig. 11); thus, aileron restraint is not indicated to have much effect on the subsonic flutter characteristics.

In order to eliminate the possibility that flap motion or camber bending of the inboard, rearward surfaces were importantly involved in the subsonic flutter mode, one run (run 36, table VI) was made with external ribs over the wing and flaps. The ribs consisted of 1/8-inch-diameter, hollow, stainless-steel rods soldered to a base of shim stock. The ribs were glued to the surfaces at the locations indicated in figure 4(h). One run (run 37, table VI) was also made with the external ribs sawed in two at the flap hinge line. These runs were made at a Mach number of about 0.9, and the results (table VI) were similar to those obtained (fig. 11) without the external ribs.

## SUMMARY OF RESULTS

The transonic flutter characteristics of models of the wing of a new fighter airplane have been studied in the Langley transonic blowdown tunnel. The wing has an arrowhead plan form, was equipped with ailerons at the tips and with flaps at the trailing edges, and was cantilever mounted. The models were dynamically and elastically scaled by criteria which provide a flutter safety margin. The margin was such that if at a given Mach number a certain altitude is cleared by the model, that Mach number and altitude could be reached with a 32-percent margin of safety in stiffness by the airplane. The following results were obtained:

1. The basic configuration was flutter free at Mach numbers from about 1.0 to 1.1 at simulated altitudes as low as sea level, but flutter was obtained at altitudes above sea level at both higher and lower Mach numbers. The flutter mode at subsonic Mach numbers involved primarily bending and torsion of the wing with little independent aileron motion. The flutter mode at supersonic Mach numbers involved primarily aileron rotation with some bending of the aileron spar, and the flutter boundary was such that a rapid decrease in the dynamic pressure required for flutter was obtained as the Mach number was increased to above a value of about 1.1.

2. In an effort to improve the flutter boundary at supersonic Mach numbers, three aileron modifications were investigated. Increases in the stiffness of the aileron spar reduced the altitude at supersonic Mach numbers at which flutter occurred. Cutting off the tip of the aileron or increasing the simulated actuator stiffness to about three times the original value eliminated flutter at supersonic Mach numbers at altitudes as low as sea level.

3. An intensive investigation of the flutter boundary at Mach numbers from about 0.85 to 0.95 was made with the ailerons of the basic configuration locked. The data obtained indicated that the flutter in this Mach number region ceases if the dynamic pressure is increased sufficiently. Aileron restraint was not indicated to have much effect on the subsonic flutter characteristics.

Langley Aeronautical Laboratory,  
National Advisory Committee for Aeronautics,  
Langley Field, Va., August 8, 1957.

## REFERENCES

1. Anon.: Standard Atmosphere - Tables and Data for Altitudes to 65,800 Feet. NACA Rep. 1235, 1955. (Supersedes NACA TN 3182.)
2. Jones, George W., Jr., and Young, Lou S., Jr.: Transonic Flutter Investigation of Two  $64^\circ$  Delta Wings With Simulated Streamwise Rib and Orthogonal Spar Construction. NACA RM L56I27, 1957.
3. Unangst, John R., and Jones, George W., Jr.: Some Effects of Sweep and Aspect Ratio on the Transonic Flutter Characteristics of a Series of Thin Cantilever Wings Having a Taper Ratio of 0.6. NACA RM L55I13a, 1956.
4. Bursnall, William J.: Initial Flutter Tests in the Langley Transonic Blowdown Tunnel and Comparison With Free-Flight Flutter Results. NACA RM L52K14, 1953.

TABLE I.- GEOMETRIC PROPERTIES OF BASIC MODELS

Streamwise airfoil section . . . . .	NACA 65A003
Leading-edge sweepback, deg . . . . .	55
Trailing-edge sweepback, deg . . . . .	10
Aileron hinge-line sweepback, deg . . . . .	4.5
Flap hinge-line sweepback, deg . . . . .	10
Panel span, ft . . . . .	0.596
Flap span, ft . . . . .	0.371
Streamwise panel root chord, ft . . . . .	0.778
Streamwise flap chord, ft . . . . .	0.122
Panel area, sq ft . . . . .	0.241
Ratio of aileron area to exposed panel area . . . . .	0.200
Ratio of flap area to exposed panel area . . . . .	0.188
Exposed panel aspect ratio . . . . .	1.47
Exposed panel taper ratio . . . . .	0.042
Fuselage diameter, ft . . . . .	0.250
Plan-form span, ft . . . . .	1.442
Maximum streamwise chord based on extension of panels to model center line, ft . . . . .	0.935
Plan-form area based on extension of panels to model center line, sq ft . . . . .	0.698
Plan-form aspect ratio based on extension of panels to model center line . . . . .	2.98
Plan-form taper ratio based on extension of panels to model center line . . . . .	0.035

TABLE II.- INDEX OF FIGURES FOR CONFIGURATIONS INVESTIGATED

Configurations	Wing	Panel	Runs	Natural-frequency figures	Flutter-data figures
Basic configuration . . .	1	Both	1 to 2	4(a)	6
Basic configuration . . .	1	Left	3 to 8	4(a)	6
Basic configuration . . .	2	Both	9	4(b)	6
Stiffened aileron spar . . . . .	2	Right	10 to 13	4(c)	7
Aileron tip cut off . . .	3	Right	14 to 17	4(d)	8
Stiffened aileron actuator . . . . .	1	Left	18 to 21	4(e)	9
Aileron having stiffened spar, tip cut off, and stiffened actuator . .	2	Left	22 to 26	4(f)	10
Aileron locked . . . . .	3	Both	27 to 35	4(g)	11
Aileron locked, external ribs over wing and flap . . . . .	3	Both	36	4(h)	None
Aileron locked, external ribs cut at flap hinge line . . . . .	3	Both	37	None	None

TABLE III.- DESIGN SCALE FACTORS OF PERTINENT WING  
AND FLOW QUANTITIES

$$\left[ \frac{\rho_M}{\rho_A} = 2.00; \frac{T_M}{T_A} = 0.786; \eta = 0.76 \right]$$

Quantity	Design scale factor	
	Symbolical	Numerical
Fundamental quantities		
Length . . . . .	$l$	0.040
Mass . . . . .	$m = \frac{\rho_M}{\rho_A} l^3$	$0.128 \times 10^{-3}$
Time . . . . .	$t = \left( \frac{T_M}{T_A} \right)^{-1/2} l$	0.045
Derived quantities		
Stream velocity . . . . .	$lt^{-1}$	0.888
Stream dynamic pressure . . . . .	$l^{-1}mt^{-2}$	1.58
Moment of inertia . . . . .	$l^2m$	$2.05 \times 10^{-7}$
$k_\beta$ . . . . .	$\eta l^2mt^{-2}$	$7.69 \times 10^{-5}$
EI and GJ . . . . .	$\eta l^3mt^{-2}$	$3.07 \times 10^{-6}$
Structural influence coefficients . . .	$\eta^{-1}m^{-1}t^2$	20.8
Natural vibration frequency . . . . .	$\eta^{1/2}t^{-1}$	19.4

TABLE IV.- STRUCTURAL INFLUENCE COEFFICIENTS FOR LEFT WING PANEL OF WING 2

(a) Measured values normalized for unit loadings,  $\frac{ft}{lb} \times 10^5$

Deflection points	Load points																	
	1	2	3	4	5	6	7	8	9	10	11	12	13	14	15	16	17	18
1	3.67	1.35	0.722	0.408	0.825	0.537	0.508	0.583	0.126	0.194	0.128	0.294	0.625	0.750	0.696	0.442	0.553	0.481
2	1.30	6.05	4.17	1.08	2.21	3.15	1.09	2.80	.492	2.12	.172	1.81	4.04	4.33	4.79	5.47	3.37	4.72
3	.695	4.08	14.2	2.27	6.96	11.1	4.11	12.8	2.75	10.6	1.90	9.75	15.5	17.3	21.6	25.6	18.2	22.4
4	.389	1.16	2.33	1.31	2.07	2.88	1.42	3.26	1.18	3.02	1.05	3.07	3.38	4.18	4.73	5.62	4.48	5.20
5	.806	2.32	6.80	2.16	8.14	11.9	5.33	14.4	5.37	14.4	5.33	15.2	16.2	18.6	23.2	27.2	21.1	27.0
6	.592	3.12	11.2	2.86	11.6	21.1	8.33	28.5	9.17	28.2	10.6	30.8	27.3	38.8	47.5	57.2	44.7	54.6
7	.508	1.10	4.05	1.47	5.37	8.58	7.02	12.3	6.49	13.4	7.55	14.3	10.0	12.7	16.8	19.7	17.2	19.5
8	.703	2.85	12.3	3.35	14.3	28.2	12.1	53.9	16.3	52.2	22.1	58.5	39.6	63.1	82.7	106	82.8	103
9	.150	.458	2.82	1.30	5.33	9.33	6.43	16.7	24.3	22.7	41.4	32.5	10.3	16.2	21.3	27.2	26.2	28.1
10	.207	2.12	10.4	3.17	14.3	28.2	13.5	53.6	22.9	122	34.9	86.7	38.2	62.2	85.8	107	90.8	107
11	.135	.167	2.01	.925	5.17	10.7	7.57	22.5	41.5	34.5	97.5	54.5	12.2	20.5	28.3	34.2	34.9	35.3
12	.285	1.78	9.75	3.11	15.2	30.7	14.2	58.2	31.8	85.0	53.6	91.7	40.2	66.5	95.0	121	104	119
13	.617	3.98	15.5	3.45	16.2	27.3	9.58	40.8	10.0	38.6	11.7	41.9	59.2	62.8	75.7	84.2	53.3	73.6
14	.821	4.37	17.2	4.05	18.7	39.6	12.2	63.5	16.5	62.6	20.6	67.2	64.7	112	153	201	136	177
15	.612	4.88	20.8	4.87	23.0	46.2	16.8	84.2	20.1	83.3	27.7	95.8	73.2	154	251	387	231	352
16	.426	5.45	24.5	5.67	27.5	55.9	19.7	106	26.2	107	33.7	120	84.2	201	374	651	339	584
17	.603	3.37	18.2	4.68	21.0	43.4	17.3	84.2	26.4	90.0	35.2	103	51.9	130	228	336	322	362
18	.459	4.76	22.0	5.37	26.8	54.7	19.1	102	26.7	103	36.3	115	72.7	177	347	582	362	588

TABLE IV.- STRUCTURAL INFLUENCE COEFFICIENTS FOR LEFT WING PANEL OF WING 2 - Concluded

(b) Symmetrical matrix,  $\frac{ft}{lb} \times 10^5$

Deflection points	Load points																	
	1	2	3	4	5	6	7	8	9	10	11	12	13	14	15	16	17	18
1	3.67	1.32	0.708	0.398	0.816	0.564	0.508	0.643	0.138	0.200	0.132	0.290	0.621	0.786	0.654	0.434	0.578	0.470
2		6.05	4.12	1.12	2.26	3.14	1.10	2.82	.475	2.12	.170	1.80	4.01	4.35	4.84	5.46	3.37	4.74
3			14.2	2.30	6.88	11.2	4.08	12.6	2.78	10.5	1.96	9.75	15.5	17.2	21.2	25.0	18.2	22.2
4				1.31	2.12	2.87	1.44	3.30	1.24	3.10	.988	3.09	3.42	4.12	4.80	5.64	4.58	5.28
5					8.14	11.8	5.35	14.4	5.35	14.4	5.25	15.2	16.2	18.6	23.1	27.4	21.0	26.9
6						21.1	8.46	28.4	9.25	28.2	10.6	30.8	27.3	39.2	46.8	56.6	44.0	54.6
7							7.02	12.2	6.46	13.4	7.56	14.2	9.79	12.4	16.8	19.7	17.2	19.3
8								53.9	16.5	52.9	22.3	58.4	40.2	63.3	83.4	106	83.5	102
9									24.3	22.8	41.4	32.2	10.2	16.4	20.7	26.7	26.3	27.4
10										122	34.7	85.8	38.4	62.4	84.6	107	90.4	105
11											97.5	54.0	12.0	20.6	28.0	34.0	35.0	35.8
12												91.7	41.0	66.8	95.4	120	104	117
13													59.2	63.8	74.4	84.2	52.6	73.2
14														112	154	201	133	177
15															251	380	230	350
16																651	338	583
17																	322	362
18																		588

TABLE V.- PROPERTIES OF STREAMWISE STRIPS OF  
 RIGHT PANEL OF WING 1  
 [Total panel mass, 0.006633 slug]

Strip	$m_s$ , slugs	$x_{cg}$ , percent chord	$I_s$ , slug-ft <sup>2</sup>	$\delta_s$ , ft	$b_s$ , ft
1	$1,426 \times 10^{-6}$	40.1	$58.3 \times 10^{-6}$	0.0800	0.362
2	1,428	60.1	65.7	.0733	.314
3	641	39.7	11.8	.0733	.268
4	1,405	54.8	30.5	.0767	.221
5	963	36.6	3.3	0.0642	0.176
6	449	48.0	2.5	.0808	.130
7	234	43.8	.6	.0758	.081
8	87	47.6	.3	.0692	.036

TABLE VI.- COMPILATION OF TEST RESULTS

Configuration	Wing	$\frac{h_p}{ft-lb}$ radian (a)		Run	Point	Panel behavior (a)		$f_p$ , cps (a)		M	$q$ , lb sq ft	$V$ , ft sec	$\rho$ , slugs cu ft	$T$ , $T_R$	$\mu$	$\frac{b_{air}}{V}$			
		Left	Right			Left	Right	Left	Right										
																	Left	Right	
Basic . . . . .	1	97	95	1	1	N	F	---	167	0.833	1,251	879	0.0032	464	20.12	0.263			
			95	1	2	F	F	---	168	---	.832	1,348	874	.0033	460	18.40	.266		
			95	1	3	E	E	---	---	---	.863	1,565	896	.0039	448	16.31	---		
			95	1	4	Q	Q	---	---	---	.853	1,693	878	.0044	441	14.63	---		
			95	2	1	N	F	---	---	---	311	1.312	2,491	1,242	.0032	373	20.12	.346	
			X	3	1	Q	X	---	---	---	X	.776	1,378	821	.0047	466	13.70	---	
			X	4	1	Q	X	---	---	---	X	.779	1,712	824	.0050	466	12.88	---	
			X	5	1	F	X	---	---	---	X	.864	1,726	911	.0042	462	15.33	.259	
			X	6	1	Q	X	---	---	---	X	1.027	2,413	1,038	.0045	425	14.31	---	
			X	7	1	Q	X	---	---	---	X	1.108	2,926	1,068	.0051	386	12.62	---	
X	8	1	F	X	---	---	---	X	1.309	2,842	1,282	.0034	399	18.94	.323				
Basic . . . . .	2	94	75	9	2	N	F	---	300	1.141	1,866	1,145	0.0028	419	23.00	0.362			
						F	X	---	307	1.184	2,249	1,164	.0033	402	19.51	.364			
Stiffened aileron spar . . . . .	2	X	126	10	1	X	Q	X	---	1.097	2,873	1,051	0.0052	382	12.38	---			
				11	1	X	D	X	---	---	---	1.192	2,158	1,173	.0031	403	20.77	---	
				11	2	X	F	X	---	---	---	395	1.218	3,130	1,162	.0046	379	14.00	0.170
				12	1	X	D	X	---	---	---	---	1.300	2,953	1,239	.0038	378	16.94	---
				12	2	X	F	X	---	---	---	---	400	1.314	3,684	1,222	.0049	360	13.14
Aileron tip cut off . . . . .	3	X	137	14	1	X	Q	X	---	1.107	2,884	1,062	0.0051	383	12.62	---			
				15	1	X	D	X	---	---	---	1.206	3,364	1,134	.0030	381	12.88	---	
				16	1	X	D	X	---	---	---	---	1.326	3,817	1,261	.0048	376	13.42	---
				16	2	X	P	X	---	---	---	400	1.336	4,196	1,250	.0054	364	11.92	0.442
				17	1	X	D	X	---	---	---	---	.890	2,619	918	.0062	443	10.38	---
Stiffer aileron actuator . . . . .	1	285	X	18	1	Q	X	---	X	1.105	2,890	1,060	0.0051	385	12.62	---			
				19	1	Q	X	---	X	---	X	1.223	3,398	1,134	.0052	364	12.38	---	
				20	1	Q	X	---	X	---	X	1.318	4,170	1,199	.0058	345	11.10	---	
				21	1	Q	X	---	X	---	X	.868	2,246	879	.0058	427	11.10	---	
				Aileron with three modifications . . . . .	2	243	X	22	1	Q	X	---	X	1.095	2,808	1,039	0.0052	375	12.38
23	1	Q	X					---	X	---	X	1.207	3,326	1,154	.0050	318	12.88	---	
24	1	Q	X					---	X	---	X	1.330	4,239	1,240	.0055	362	11.71	---	
25	1	F	X					---	---	---	---	167	X	.868	906	.0043	453	14.97	0.255
26	1	Q	X					---	X	---	X	1.360	4,205	1,197	.0058	349	11.10	---	
Locked aileron . . . . .	3	"	"	27	1	F	F	155	155	0.904	1,191	961	0.0026	471	24.77	0.223			
				27	2	E	E	---	---	---	---	.928	1,256	983	.0026	467	24.77	---	
				27	3	Q	Q	---	---	---	---	1.106	3,879	1,054	.0070	378	9.20	---	
				28	1	F	F	171	171	---	---	.857	1,444	915	.0034	474	18.94	.258	
				28	2	E	E	---	---	---	---	.856	1,541	911	.0037	471	17.40	---	
				28	3	Q	Q	---	---	---	---	.886	3,237	883	.0033	413	7.76	---	
				29	1	Q	Q	---	---	---	---	1.352	4,228	1,274	.0052	381	12.38	---	
				30	1	F	F	168	168	---	---	.881	1,333	928	.0031	461	20.77	.250	
				30	2	E	E	---	---	---	---	.928	1,593	965	.0034	450	18.94	---	
				30	3	Q	Q	---	---	---	---	.973	2,271	974	.0048	417	13.42	---	
				31	1	F	F	168	168	---	---	.830	1,405	882	.0036	470	17.89	.263	
				31	2	E	E	---	---	---	---	.854	1,807	891	.0045	453	14.31	---	
				31	3	Q	Q	---	---	---	---	.864	2,020	890	.0051	441	12.62	---	
				32	1	F	F	169	169	---	---	.883	1,297	932	.0030	464	21.46	.251	
				32	2	E	E	---	---	---	---	.921	1,526	962	.0033	454	19.51	---	
				32	3	Q	Q	---	---	---	---	.973	2,271	973	.0048	416	13.42	---	
				33	1	F	F	160	160	---	---	.913	1,293	964	.0028	464	23.00	.229	
				33	2	E	E	---	---	---	---	.934	1,366	983	.0028	461	23.00	---	
				33	3	Q	Q	---	---	---	---	1.021	1,855	1,047	.0034	438	18.94	---	
				34	1	F	F	169	169	---	---	.874	1,512	920	.0036	462	17.89	.254	
34	2	E	E	---	---	---	---	.895	1,747	932	.0040	452	16.10	---					
34	3	Q	Q	---	---	---	---	.895	2,349	877	.0061	400	10.36	---					
35	1	F	F	---	---	---	---	1.246	3,574	1,186	.0051	377	12.62	---					
Locked aileron, external ribs . . . . .	3	"	"	36	1	F	F	169	169	0.864	1,469	905	0.0036	457	17.89	0.258			
				36	2	E	E	---	---	---	---	.895	2,105	922	.0032	432	12.38	---	
				36	3	Q	Q	---	---	---	---	.872	2,271	876	.0059	420	10.91	---	
Locked ailerons, cut external ribs . . . . .	3	"	"	37	1	F	F	168	168	0.861	1,411	892	0.0035	447	18.40	0.260			
				37	2	E	E	---	---	---	---	.891	1,735	912	.0042	436	15.33	---	

<sup>a</sup>Panel-behavior code: N, no flutter; D, start of low damping; F, start of flutter or continuation of flutter; E, end of flutter; Q, maximum q, no flutter; X, aileron inoperative.

Note: All dimensions in inches  
 --- Axis about which  $I_g$  was measured (Table V)  
 ⊙ Strip center of gravity

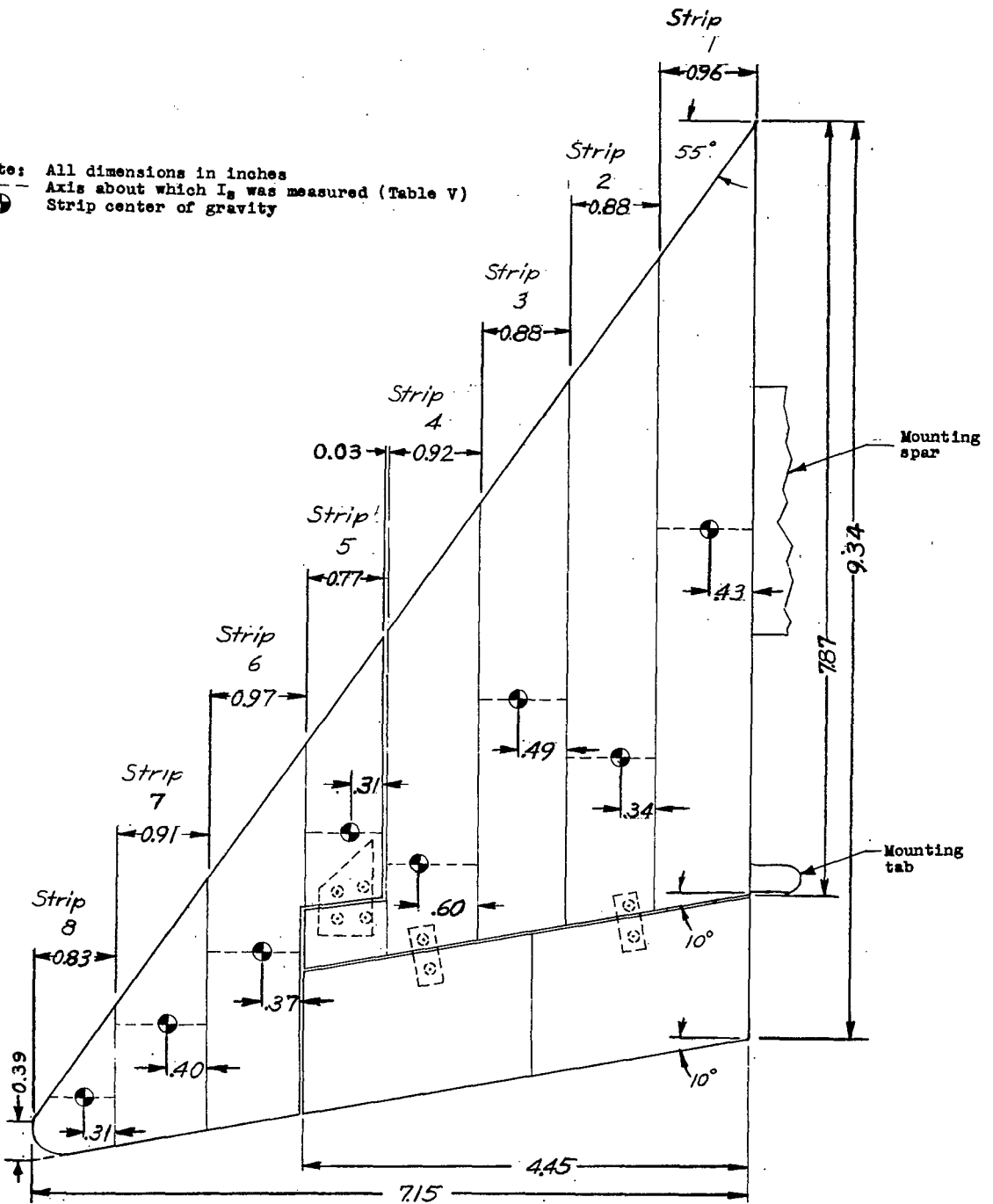
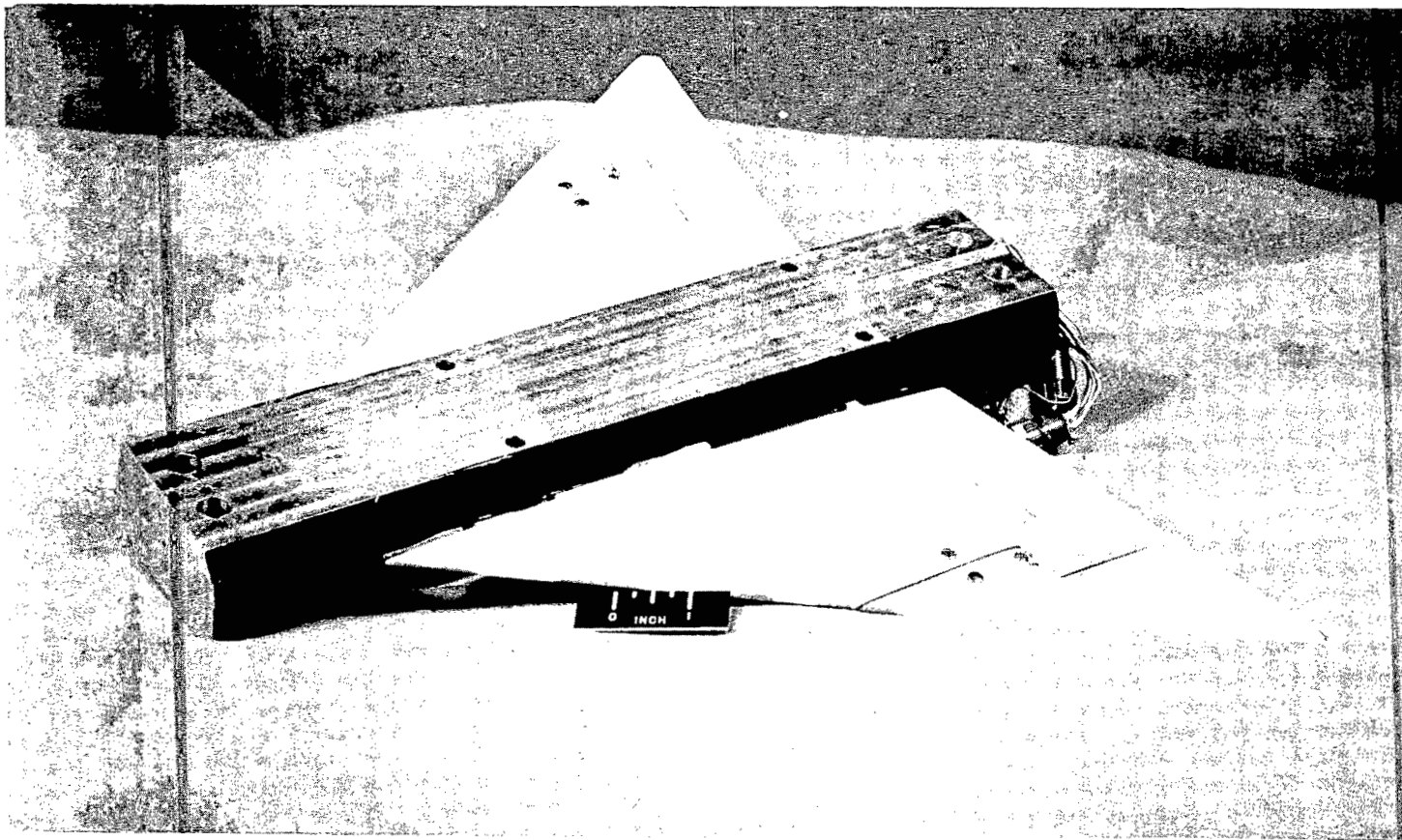
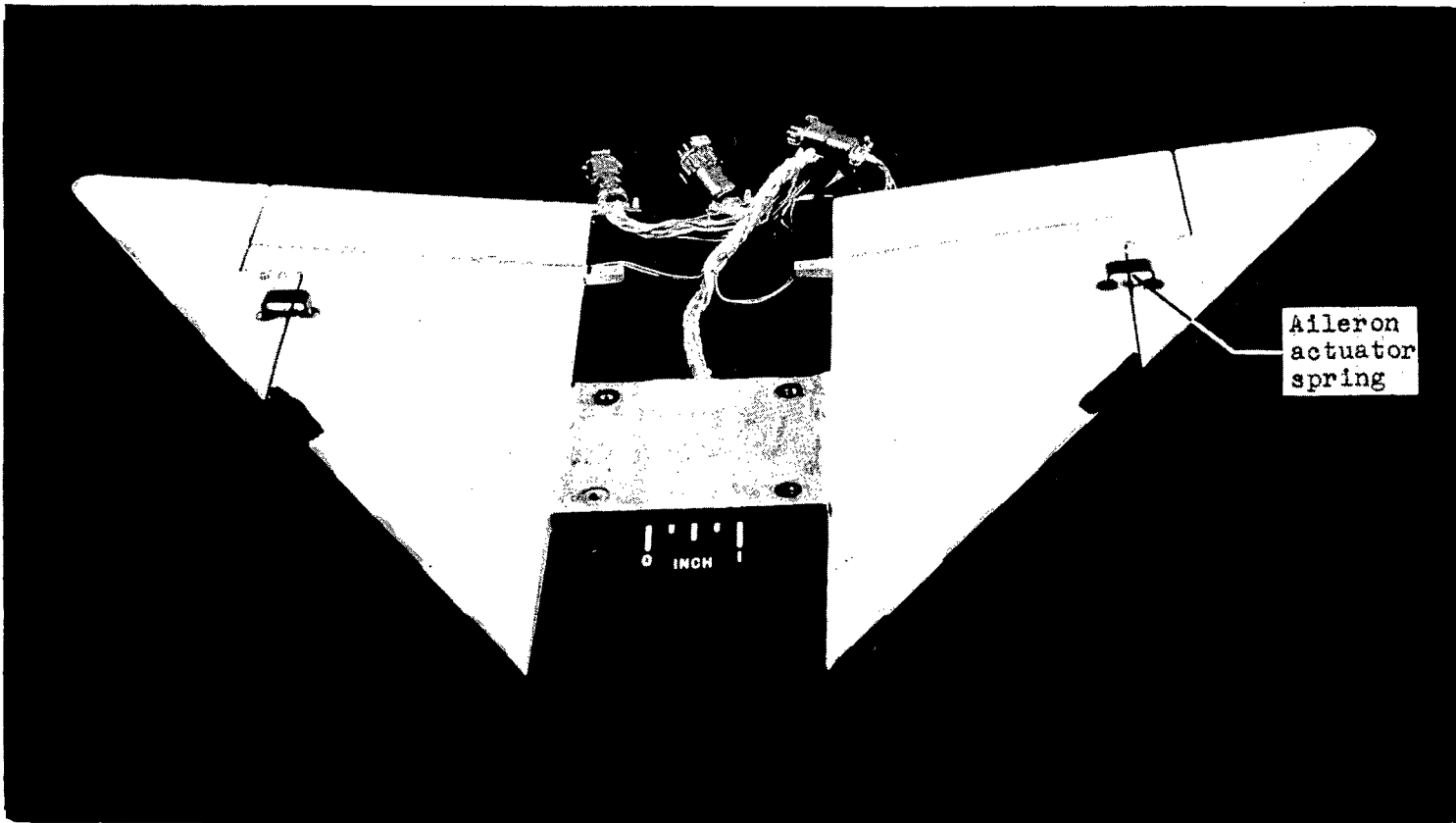


Figure 1.- Model dimensions.



(a) Top view of model in mounting block. L-95307

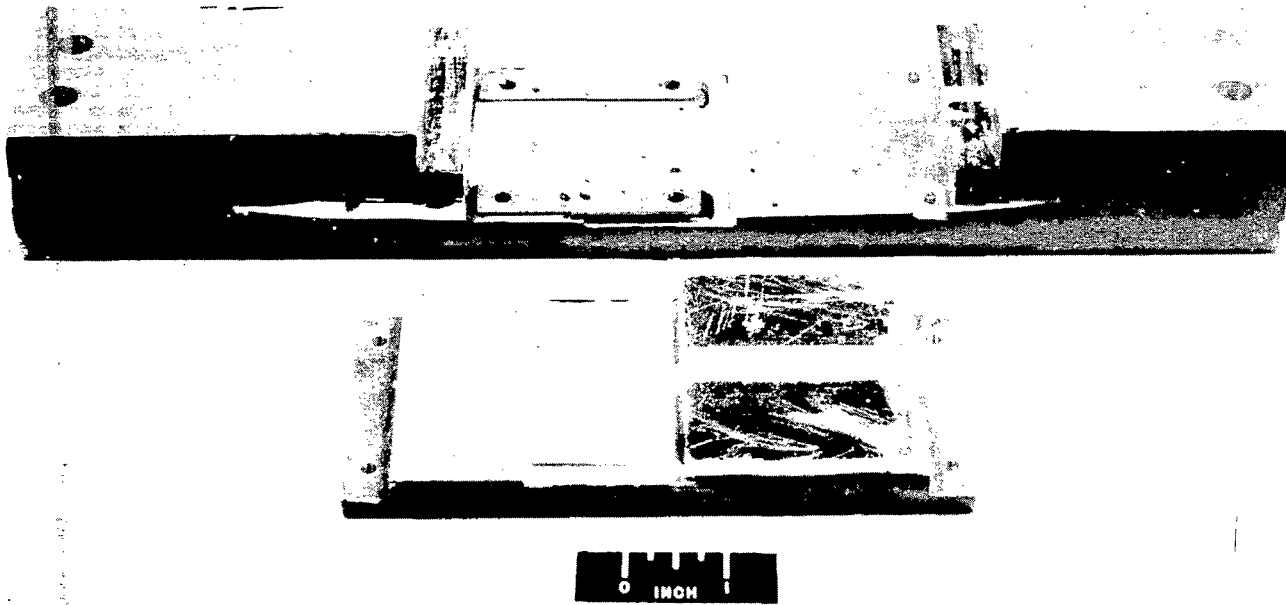
Figure 2.- Photographs of basic model and of mounting block.



(b) Bottom view of model.

L-95309.1

Figure 2.- Continued.



(c) View of mounting block.

L-95310

Figure 2.- Concluded.

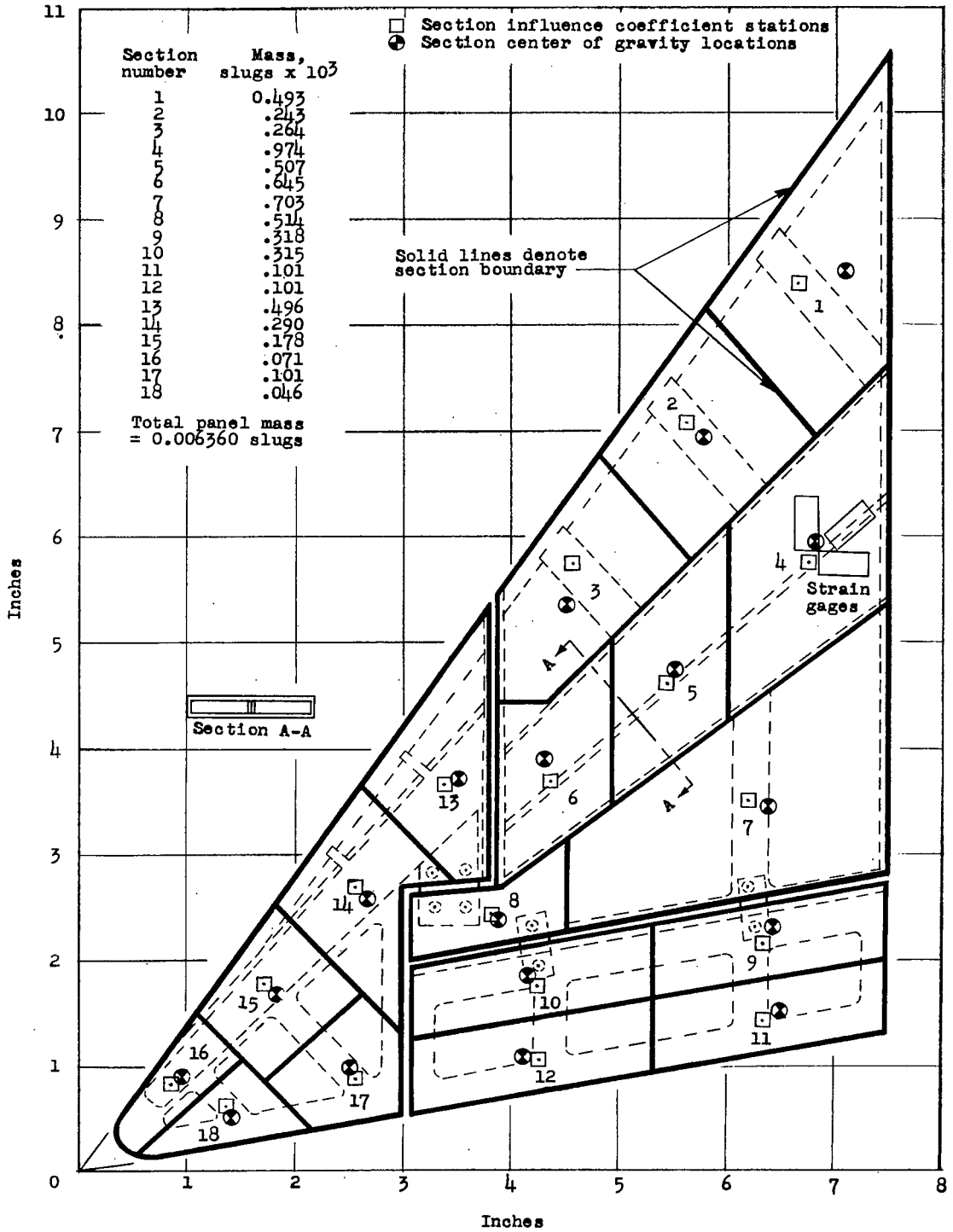
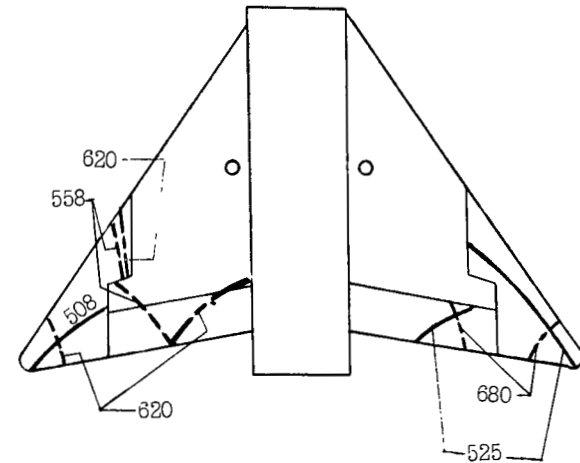
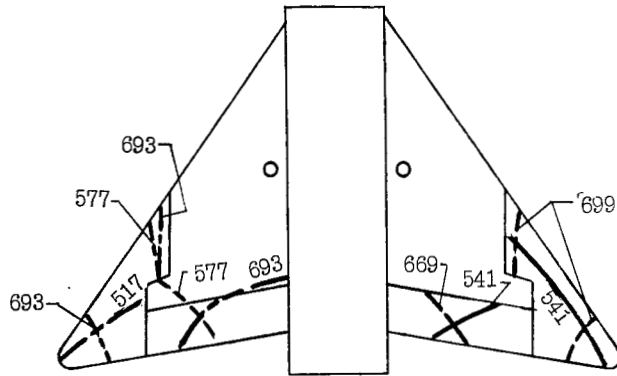
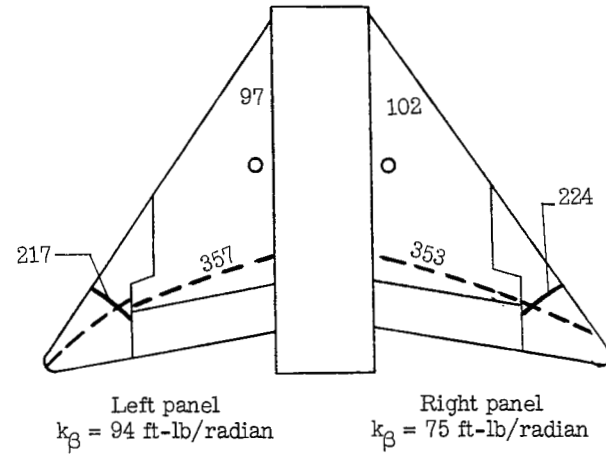
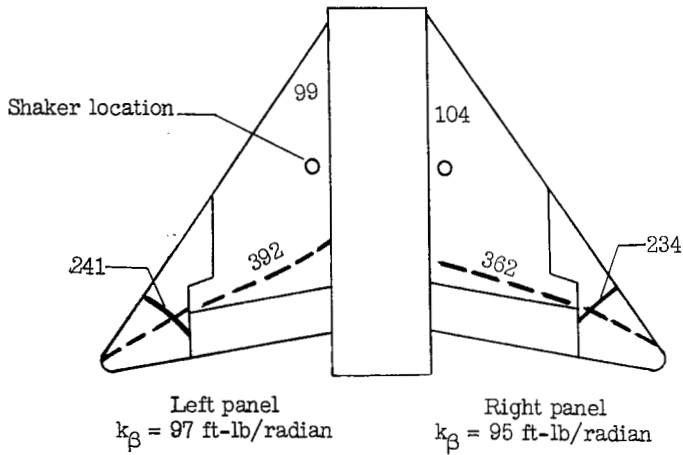


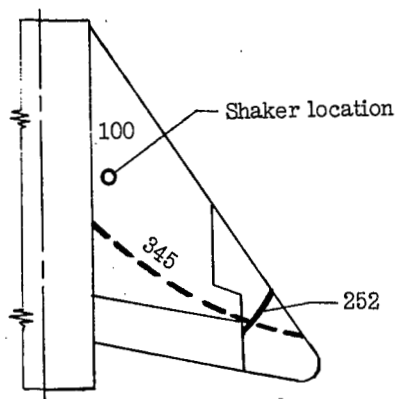
Figure 3.- Model construction and influence-coefficient stations.



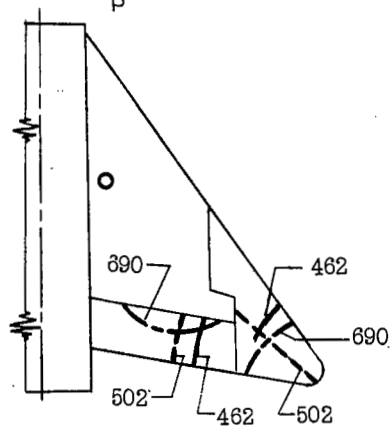
(a) Basic configuration. Wing 1.

(b) Basic configuration. Wing 2.

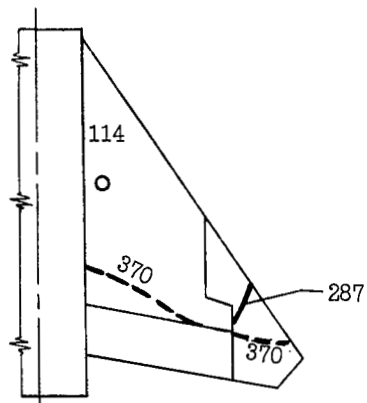
Figure 4.- Measured model frequencies, node lines, and aileron-spring constants.



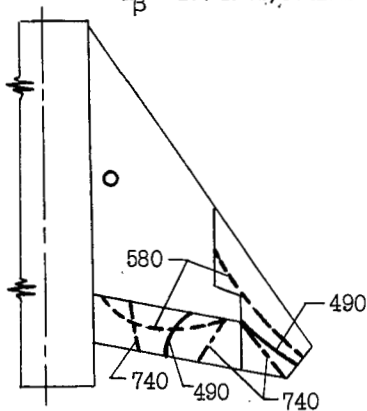
Right panel  
 $k_{\beta} = 126 \text{ ft-lb/radian}$



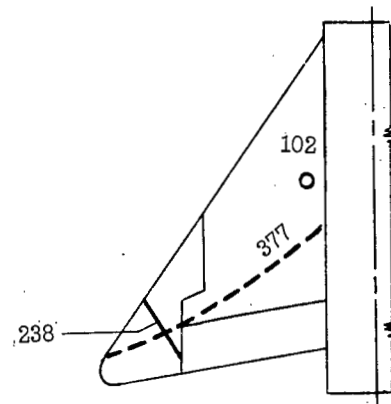
(c) Stiffened aileron spar.  
 Wing 2.



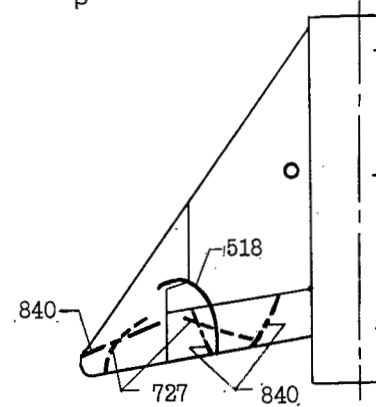
Right panel  
 $k_{\beta} = 137 \text{ ft-lb/radian}$



(d) Aileron tip cut off.  
 Wing 3.

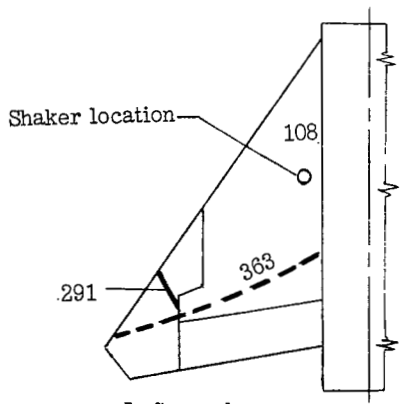


Left panel  
 $k_{\beta} = 285 \text{ ft-lb/radian}$

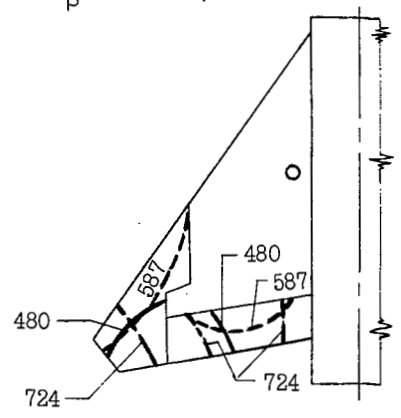


(e) Stiffened aileron actuator.  
 Wing 1.

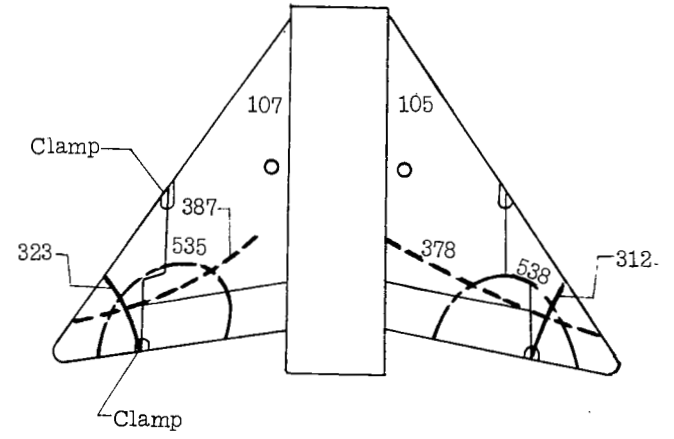
Figure 4.- Continued.



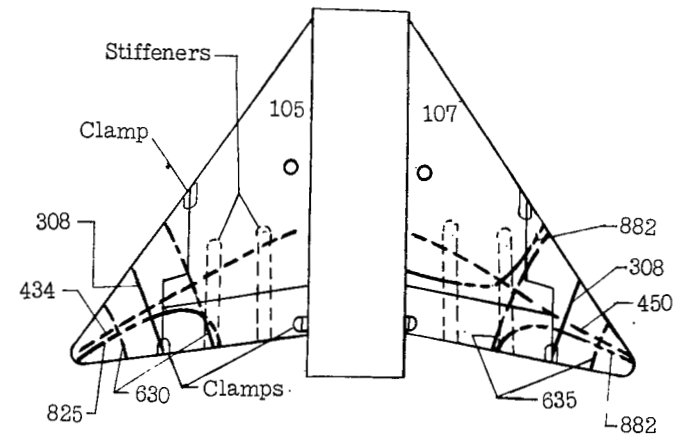
Left panel  
 $k_B = 243 \text{ ft-lb/radian}$



(f) Stiffened aileron spar, aileron tip cut off, and stiffened aileron actuator. Wing 2.



(g) Ailerons glued to wing. Wing 3.



(h) Ailerons glued to wing and external ribs installed over flaps. Wing 3.

Figure 4.- Concluded.

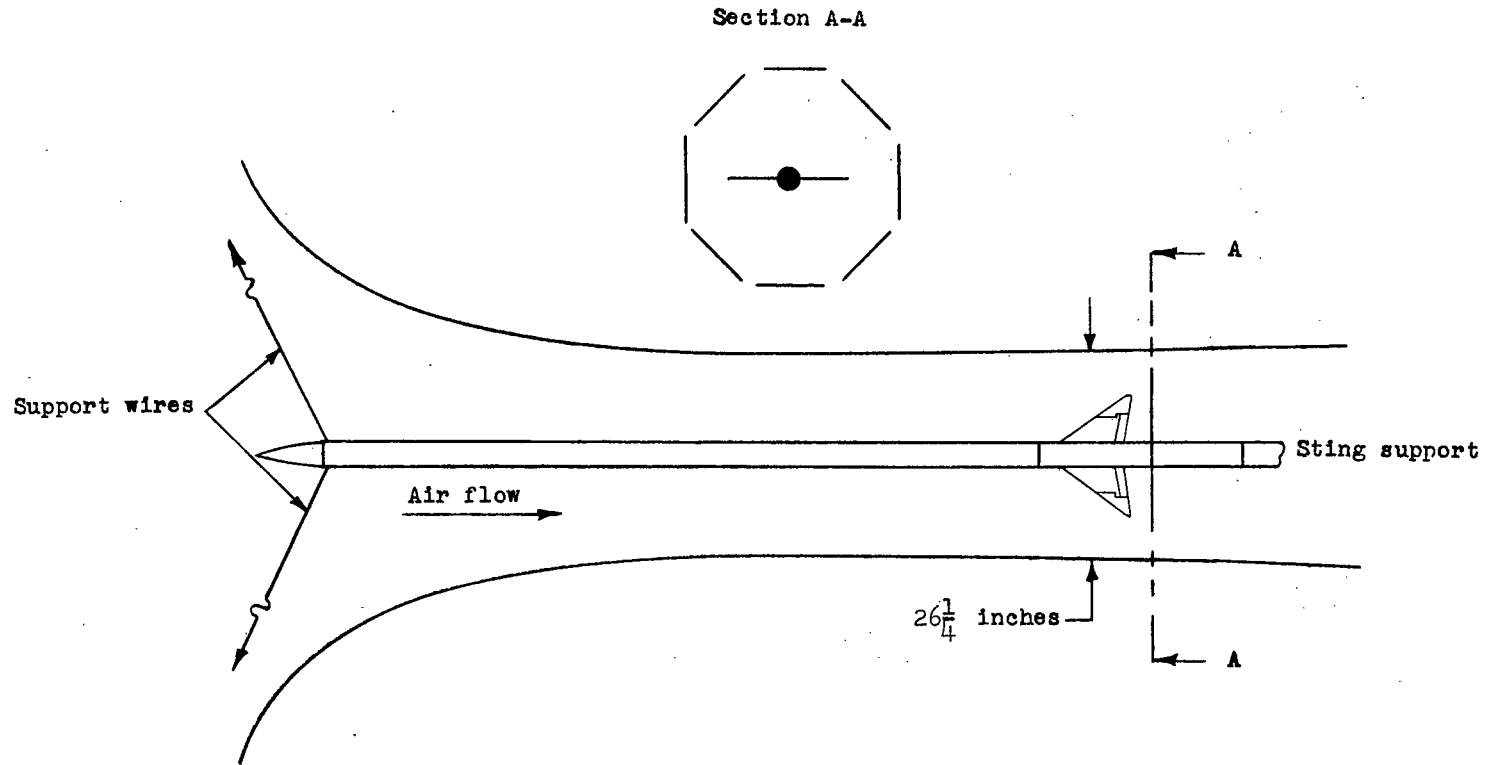


Figure 5.- Sketch of model mounted on sting and installed in tunnel.

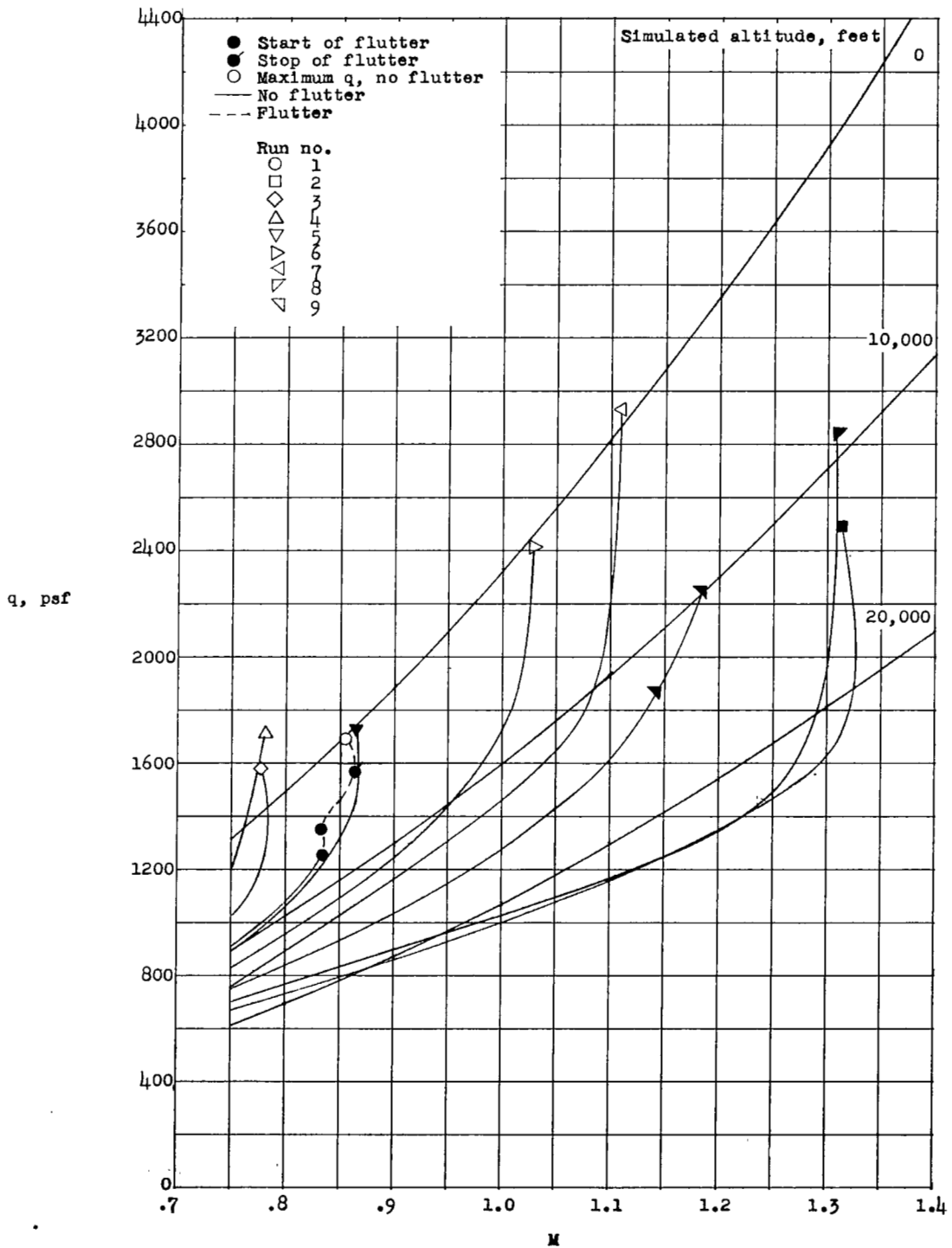


Figure 6.- Flutter characteristics of basic-wing configuration.

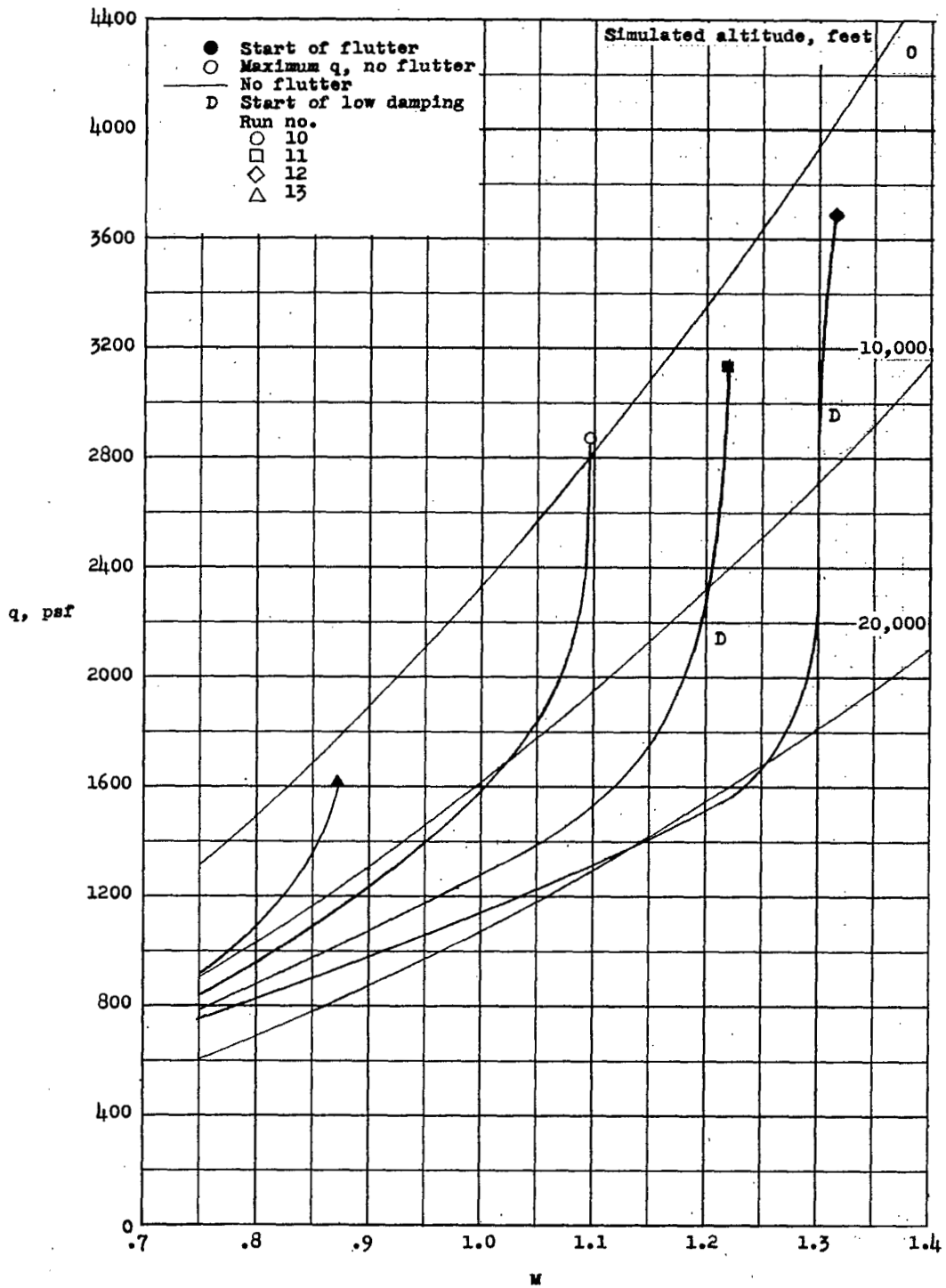


Figure 7.- Flutter characteristics of wing with stiffened aileron spar.

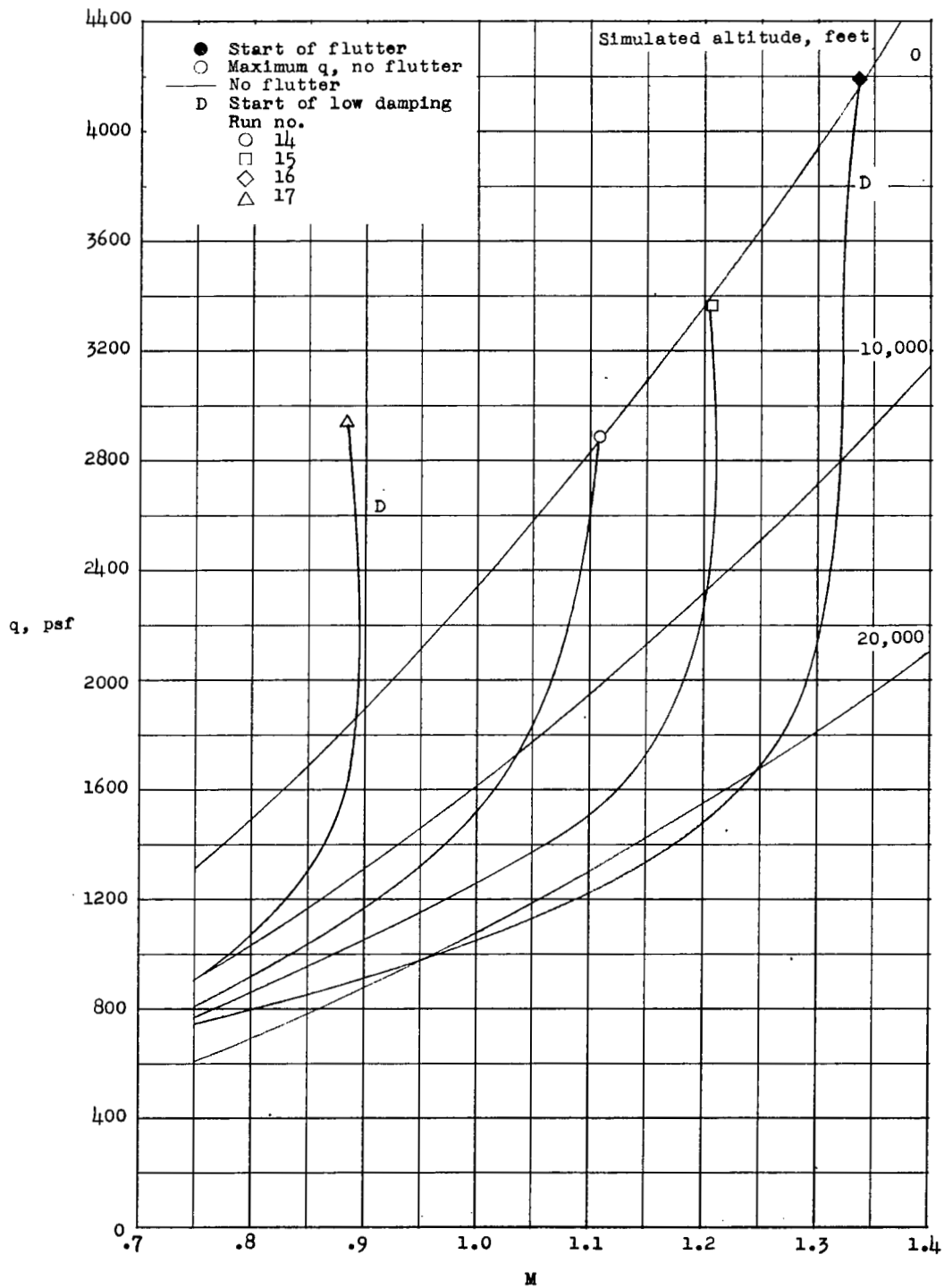


Figure 8.- Flutter characteristics of wing with aileron tip cut off.

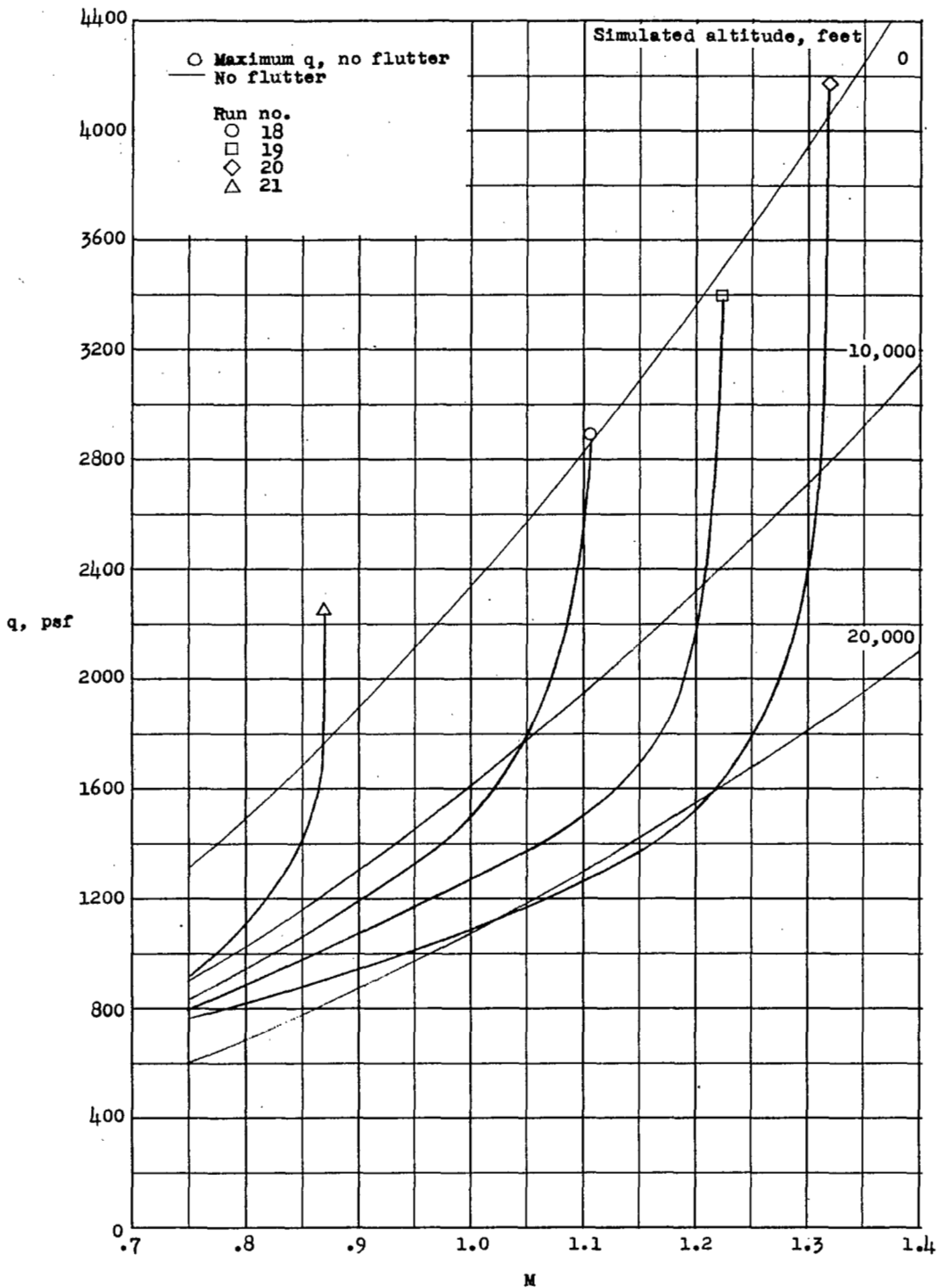


Figure 9.- Flutter characteristics of wing with increased aileron-actuator stiffness.

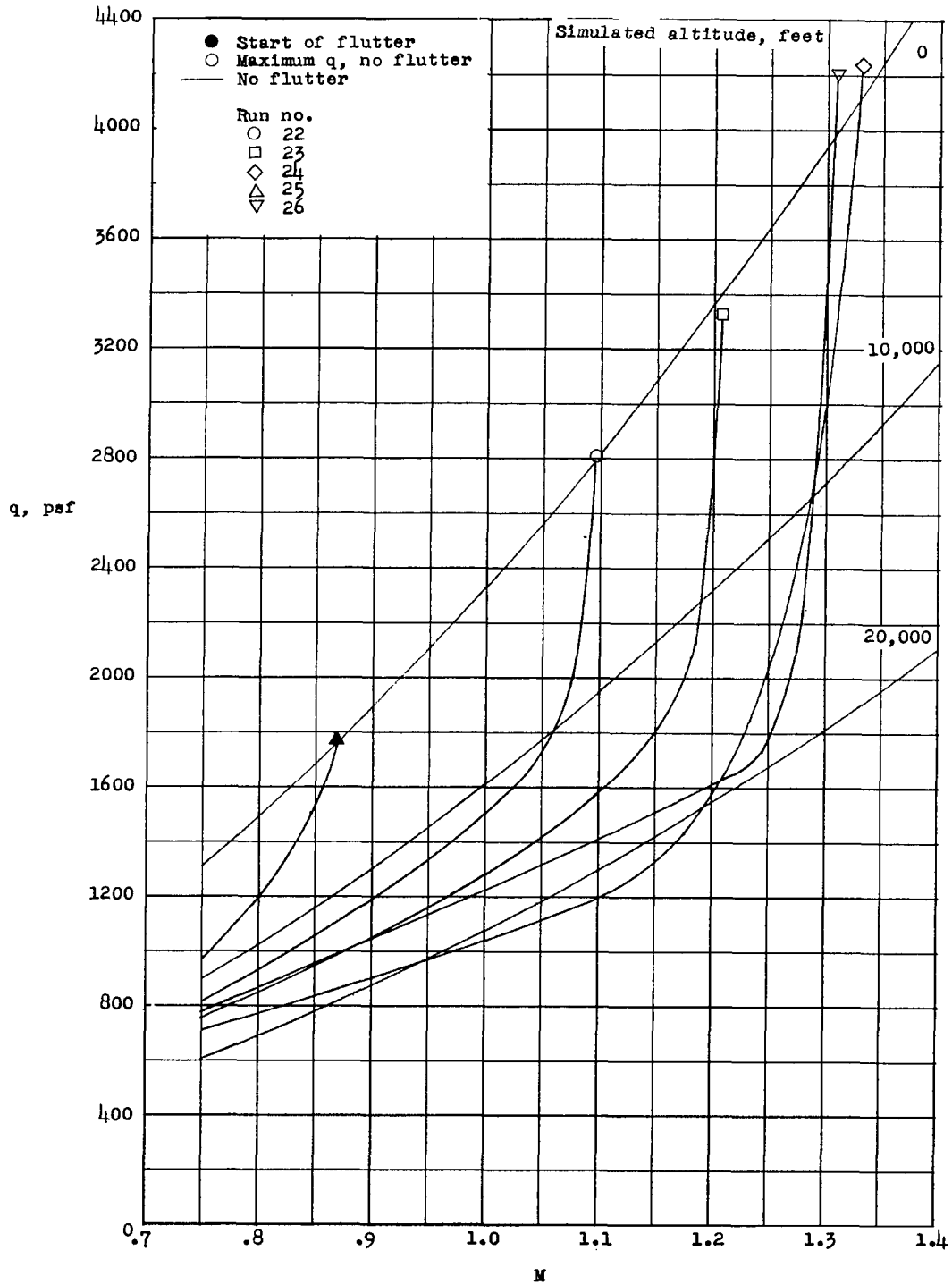


Figure 10.- Flutter characteristics of wing with stiffened aileron spar, aileron tip cut off, and increased aileron-actuator stiffness.

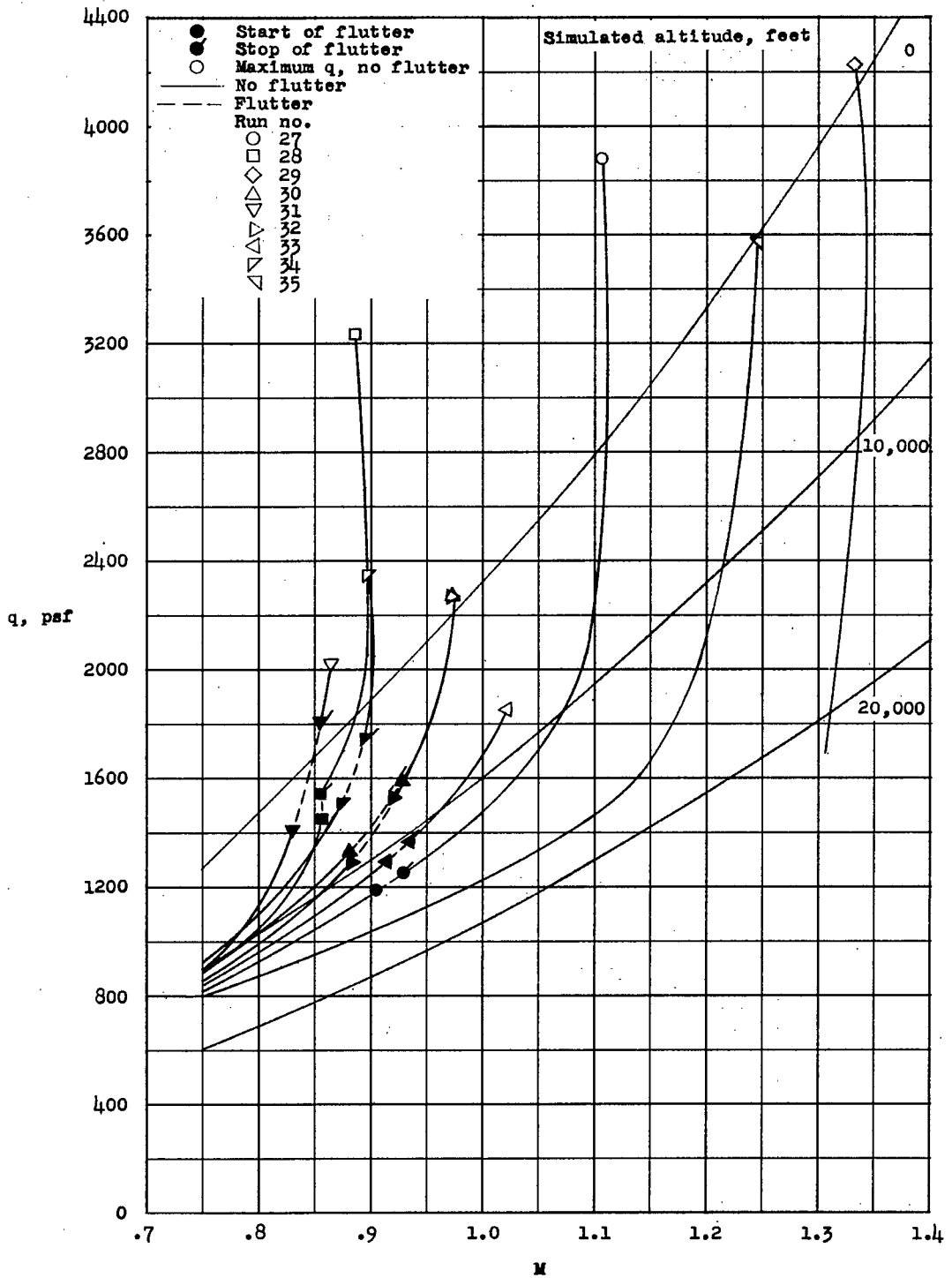
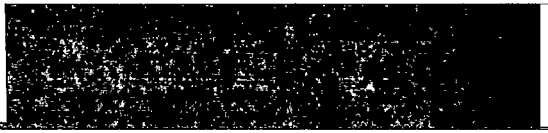


Figure 11.- Flutter characteristics of wing with aileron locked.

NASA Technical Library



3 1176 01437 2495



**CONFIDENTIAL**